

Deterministic interconversion of GHZ state and KLM state via Lie-transform-based pulse design in Rydberg atoms

J. P. Wang,¹ Y. Q. Ji,^{1,*} L. P. Yang,¹ C. Q. Wang,¹ L. Dong,¹ and X. M. Xiu^{1,†}

¹College of Physical Science and Technology, Bohai University, Jinzhou 121013, China

(Dated: May 27, 2024)

Conversion between different types of entangled states is an interesting problem in quantum mechanics. But research on the conversion between Greenberger-Horne-Zeilinger (GHZ) state and Knill-Laflamme-Milburn (KLM) state in atomic system is absent. In this paper, we propose a scheme to realize the interconversion (one-step) between GHZ state and KLM state with Rydberg atoms. By utilizing Rydberg-mediated interactions, we simplify the system. By combining Lie-transform-based pulse design, the evolution path is built up to realize interconversion of GHZ state and KLM state. The numerical simulation result shows that the present scheme is robust against decoherence and operational imperfection, the analysis shows that the scheme is feasible with current experimental technology.

I. INTRODUCING

Quantum entanglement [1, 2] is one of the most fascinating phenomena in quantum mechanics. Entangled states are useful for exploring non-locality, bolstering quantum mechanics against theories of local hidden variables. Moreover, entangled states also are key resource for quantum information processing tasks. It is widely used in quantum teleportation [3, 4], quantum key distribution [5, 6], quantum cryptography [2, 7–9], quantum computing [10–12] and so on. So far, many theoretical and experimental schemes have been proposed for preparing and converting entangled states [13–23]. As we know, each type of entangled state has its own characteristics, therefore, exploring the conversion between different types of entangled states has become a fascinating research direction in quantum mechanics.

On the other hand, neutral atoms are regarded as ideal candidates for quantum information processing due to stabilized atomic hyperfine energy states and extremely large dipole moments, which are particularly suitable for encoding logic quantum bits [24–26]. When an atom is excited to the high Rydberg state, the strong dipole-dipole interaction or van der Waals interaction will significantly shift its surrounding atomic energy levels of Rydberg states, this leads to the emergent energy level shift term in the Hamiltonian. Mathematically, it is because of this energy level shift term that a series of interesting physical phenomena arise, such as the Rydberg blocking effect [27–29] and the Rydberg anti-blocking effect [30–32]. In addition, it can be a very interesting tool to simplify the dynamics of systems, as well as, provides researchers with brand new idea. There are a lot of excellent studies to realize conversions between difference entangled state using neutral atoms [13–15, 33, 34]. It is worth noting that Zheng *et al.* [13] proposed a protocol for the one-step interconversion between GHZ state and the W state with deterministic success probabilities by utilizing Rydberg-mechanism to structure nonlocal operation. It has

been demonstrated that the two types of entangled states cannot be interconverted only by local operations and classical communication. We consider that since a deterministic interconversion between GHZ and W states can be realized in one step by utilizing Rydberg-mechanism to structure non-local operation [13], it might also be possible to realize the deterministic conversion between other entangled states in one step.

We focus on another type of Knill-Laflamme-Milburn (KLM) entangled state [35]. The KLM state was introduced mainly in the linear optical quantum computing scheme proposed by Knill, Laflamme and Milburn. It can effectively reduce the operation error rate and improve the implementation efficiency of quantum algorithms. Since then, considerable efforts have been invested in preparing KLM-type quantum entanglement using various physical platforms [36–42], such as linear optics, atom-cavity quantum electrodynamics, nonlinear cross-Kerr mediums, and artificial atoms. The n -qubit KLM state is expressed as

$$|KLM\rangle = \sum_{k=0}^n \alpha_n |1\rangle^k |0\rangle^{n-k} \quad (1)$$

where $\alpha_n = 1/\sqrt{n+1}$, is the normalization coefficient for maximal entanglement.

After extensive literature review, although many schemes have been proposed for directly preparing GHZ state or KLM state in atomic system [20, 41–45] and a scheme for converting GHZ state and KLM state in optical systems [23], we found that research on the conversion between GHZ state and KLM state in neutral atomic systems is lacking. In the present work, inspired by the previous schemes, we propose a scheme to deterministic implement interconversion between GHZ state and KLM state with one-step. The scheme's physical model features three neutral atoms with Rydberg capabilities, positioned in a triangular configuration, the original Hamiltonian is simplified to an effective four-energy system through a meticulously crafted detunings and approximation technique. Then, we combine the effective Hamiltonian and Lie-transform-based pulse design [46] to realize the interconversion of GHZ state and KLM state.

The paper is organized as follows. In Section II, we introduce the physical model and simplify the system to an ef-

* E-mail: jiyangqiang@qymail.bhu.edu.cn

† E-mail: xiuxiaomingdl@126.com

fective four energy level system. In Section III, we briefly review the methods for Lie-transform-based pulse design, subsequently, we combine effective Hamiltonian and Lie-transform-based pulse design to structure control pulses to realize the interconversion between GHZ state and KLM state. Next, in Section IV, we give the numerical simulations and analyses for the scheme, and further discuss the robustness about a number of imperfections. At last, a summary is given in Section V.

II. PHYSICAL MODEL

We consider three same neutral atoms confined within three distinct microscopic dipole traps, and arranged in a triangular configuration as show in Fig.1(a), V represents the van der Waals or dipole-dipole interaction between different atoms that are in Rydberg states. The energy levels of the three neutral atoms with Rydberg states as shown in Fig.1(b), each atomic level includes a ground states $|0\rangle$ and a Rydberg state $|r\rangle$. The transition $|0\rangle_k \leftrightarrow |r\rangle_k$ is driven by classical laser fields with Rabi frequencies Ω_k , whose detunings are δ_k , where k denotes the k th atom in the physical model. In the interaction picture, the Hamiltonian of the physical model takes the form($\hbar = 1$)

$$H(t) = \sum_{k=1}^3 \Omega_k e^{-i\delta_k t} |r\rangle_k \langle 0| + \text{H.c.} + V \sum_{k=2}^3 \sum_{k'=1}^{k-1} |rr\rangle_{k'k} \langle rr|. \quad (2)$$

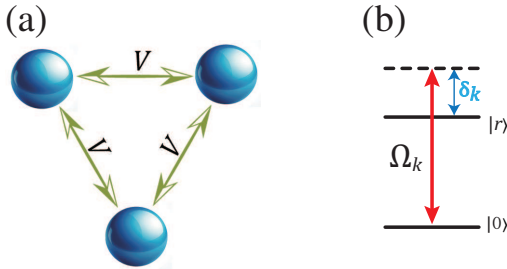


FIG. 1: (a) Schematic illustration of system. Three identical neutral atoms confined within three separate microscopic dipole traps, arranged in a triangular configuration. (b) The energy levels configuration for the single atom.

To improve understanding and facilitate discussion of the physical model, we rewrite the Hamiltonian in triatomic ba-

sis vectors

$$H = \Omega_1 e^{-i\delta_1 t} |r00\rangle \langle 000| + \Omega_2 e^{-i\delta_2 t} |0r0\rangle \langle 000| + \Omega_3 e^{-i\delta_3 t} |00r\rangle \langle 000| + \Omega_2 e^{-i\delta_2 t} |rr0\rangle \langle r00| + \Omega_3 e^{-i\delta_3 t} |r0r\rangle \langle r00| + \Omega_1 e^{-i\delta_1 t} |rr0\rangle \langle 0r0| + \Omega_3 e^{-i\delta_3 t} |0rr\rangle \langle r00| + \Omega_1 e^{-i\delta_1 t} |r0r\rangle \langle 00r| + \Omega_2 e^{-i\delta_2 t} |0rr\rangle \langle 00r| + \Omega_3 e^{-i\delta_3 t} |rrr\rangle \langle rr0| + \Omega_2 e^{-i\delta_2 t} |rrr\rangle \langle r0r| + \Omega_1 e^{-i\delta_1 t} |rrr\rangle \langle 0rr| + \text{H.c.} + V |rr0\rangle \langle rr0| + V |r0r\rangle \langle r0r| + V |0rr\rangle \langle 0rr| + 3V |rrr\rangle \langle rrr|. \quad (3)$$

From Eq.(3), we can easily observe the energy level shifts caused by Rydberg states, this energy level shift is

$$H_V = V |rr0\rangle \langle rr0| + V |r0r\rangle \langle r0r| + V |0rr\rangle \langle 0rr| + 3V |rrr\rangle \langle rrr|. \quad (4)$$

Next, we define a rotating frame with a unitary operator $\mathcal{R} = \exp(-iH_V t)$, and move into the new picture through

$$H' = \mathcal{R}^\dagger H \mathcal{R} - i\mathcal{R}^\dagger \dot{\mathcal{R}}. \quad (5)$$

So, the Hamiltonian (3) in new picture becomes

$$H' = \Omega_1 e^{-i\delta_1 t} |r00\rangle \langle 000| + \Omega_2 e^{-i\delta_2 t} |0r0\rangle \langle 000| + \Omega_3 e^{-i\delta_3 t} |00r\rangle \langle 000| + \Omega_2 e^{-i(\delta_2 - V)t} |rr0\rangle \langle r00| + \Omega_3 e^{-i(\delta_3 - V)t} |r0r\rangle \langle r00| + \Omega_1 e^{-i(\delta_1 - V)t} |rr0\rangle \langle 0r0| + \Omega_3 e^{-i(\delta_3 - V)t} |0rr\rangle \langle r00| + \Omega_1 e^{-i(\delta_1 - V)t} |r0r\rangle \langle 00r| + \Omega_2 e^{-i(\delta_2 - V)t} |0rr\rangle \langle 00r| + \Omega_3 e^{-i(\delta_3 - 2V)t} |rrr\rangle \langle rr0| + \Omega_2 e^{-i(\delta_2 - 2V)t} |rrr\rangle \langle r0r| + \Omega_1 e^{-i(\delta_1 - 2V)t} |rrr\rangle \langle 0rr| + \text{H.c.} \quad (6)$$

If we encode the logical ‘0’ with ground state $|0\rangle$ and use the Rydberg state $|r\rangle$ to encode logical ‘1’, the three-particle KLM state and GHZ state has the following form

$$|KLM\rangle = \frac{1}{2}(|000\rangle + |r00\rangle + |rr0\rangle + |rrr\rangle), \quad (7)$$

and

$$|GHZ\rangle = \frac{1}{\sqrt{2}}(|000\rangle + |rrr\rangle). \quad (8)$$

We considered that if constructing an evolutionary space within $\{|000\rangle, |r00\rangle, |rr0\rangle, |rrr\rangle\}$ from Eq.(6), it may accomplish the preparation of GHZ state and KLM state, as well as enable their interconversion. Based on this consideration, we set the detuning of the Rabi frequencies are $\delta_1 = 0$, $\delta_2 = V$, $\delta_3 = 2V$, respectively, then the Hamiltonian (6) becomes

$$H' = \Omega_1 |r00\rangle \langle 000| + \Omega_2 e^{-iVt} |0r0\rangle \langle 000| + \Omega_3 e^{-i2Vt} |00r\rangle \langle 000| + \Omega_2 |rr0\rangle \langle r00| + \Omega_3 e^{-iVt} |r0r\rangle \langle r00| + \Omega_1 e^{iVt} |rr0\rangle \langle 0r0| + \Omega_3 e^{-iVt} |0rr\rangle \langle r00| + \Omega_1 e^{iVt} |r0r\rangle \langle 00r| + \Omega_2 |0rr\rangle \langle 00r| + \Omega_3 |rrr\rangle \langle rr0| + \Omega_2 e^{iVt} |rrr\rangle \langle r0r| + \Omega_1 e^{i2Vt} |rrr\rangle \langle 0rr| + \text{H.c.} \quad (9)$$

Through neglecting highly frequent oscillations under the condition $V \gg \text{Max}\{\Omega_1, \Omega_2, \Omega_3\}$, the effective Hamiltonian is simplified as

$$H'_{eff} = \Omega_1 |r00\rangle\langle 000| + \Omega_2 |rr0\rangle\langle r00| + \Omega_2 |0rr\rangle\langle 00r| + \Omega_3 |rrr\rangle\langle rrr| + \text{H.c.} \quad (10)$$

From Eq.(10), we can find that if the initial state belongs to the evolutionary subspace $\{|000\rangle, |r00\rangle, |rr0\rangle, |rrr\rangle\}$, the evolution of the system will remain within this evolutionary subspace. That is to say, in this case, the term $\Omega_2 |0rr\rangle\langle 00r|$ and its Hermitian conjugate are decoupled in effective Hamiltonian(10), so the effective Hamiltonian becomes

$$H_{eff} = \Omega_1 |r00\rangle\langle 000| + \Omega_2 |rr0\rangle\langle r00| + \Omega_3 |rrr\rangle\langle rrr| + \text{H.c.} \quad (11)$$

III. CONTROL FIELD DESIGN THROUGH INVERSE HAMILTONIAN ENGINEERING BASED ON LIE TRANSFORMS

A. Lie-transforms-based pulse design

First of all, we briefly describe the Lie-transforms-based pulse design [46], for a quantum system with time-dependent interaction, assuming the Hamiltonian is expressed as follows

$$\mathcal{H}(t) = \sum_{j=1}^N \lambda_j(t) A_j, \quad (12)$$

where the parameters $\lambda_j(t)$ are time-dependent. Additionally, $\{A_j\}$ is a set of Hermitian generators spanning a Lie algebra and $\{A_j\}$ as the basis of an N -dimensional Hilbert space \mathcal{A} . A set of Lie transforms $\{\mathcal{L}_j\}$ is defined and each function \mathcal{L}_j acting on any vector $A \in \mathcal{A}$ is

$$\mathcal{L}_j(A) = e^{i\theta_j(t)A_j} A e^{-i\theta_j(t)A_j}, \quad (13)$$

where parameter θ_j is time-dependent and designed. Since the rotation $e^{i\theta_j(t)A_j}$ can transform the Hamiltonian from a picture to another picture, it define a picture transform \mathcal{P}_j acting on $\mathcal{H}(t)$ as

$$\begin{aligned} \mathcal{P}_j(\mathcal{H}) &= e^{i\theta_j(t)A_j} \mathcal{H}(t) e^{-i\theta_j(t)A_j} \\ &\quad - i e^{i\theta_j(t)A_j} \frac{d}{dt} \left(e^{-i\theta_j(t)A_j} \right) \\ &= \mathcal{L}_j(\mathcal{H}) - \dot{\theta}_j(t) A_j, \end{aligned} \quad (14)$$

hence, when considering the compound picture transform $\mathcal{P}_N \circ \dots \circ \mathcal{P}_2 \circ \mathcal{P}_1$ on Hamiltonian \mathcal{H} , it can obtain the

equation

$$\begin{aligned} \mathcal{P}_N \circ \dots \circ \mathcal{P}_2 \circ \mathcal{P}_1(\mathcal{H}) &= \mathcal{L}_N \circ \dots \circ \mathcal{L}_2 \circ \mathcal{L}_1(\mathcal{H}) \\ &\quad - \dot{\theta}_1 \mathcal{L}_N \circ \dots \circ \mathcal{L}_3 \circ \mathcal{L}_2(A_1) \\ &\quad - \dot{\theta}_2 \mathcal{L}_N \circ \dots \circ \mathcal{L}_4 \circ \mathcal{L}_3(A_2) \\ &\quad - \dots \\ &\quad - \dot{\theta}_{N-2}(t) \mathcal{L}_N \circ \mathcal{L}_{N-1}(A_{N-2}) \\ &\quad - \dot{\theta}_{N-1}(t) \mathcal{L}_N(A_{N-1}) \\ &\quad - \dot{\theta}_N(t) A_N. \end{aligned} \quad (15)$$

It can be observed that Eq.(15), there are N parameters $\{\theta_1, \theta_2, \dots, \theta_N\}$, corresponding to N control parameters $\{\lambda_1, \lambda_2, \dots, \lambda_n\}$, it opens up the possibility for designing control parameters.

On the other hand, quantum state evolving from the initial state $\psi(t_0)$ is controlled by the evolution operator U and satisfy the Schrödinger equation

$$i \frac{\partial}{\partial t} (U \psi(t_0)) = \mathcal{H} U \psi(t_0). \quad (16)$$

Since arbitrariness of $\psi(t_0)$, we can obtain

$$i \dot{U} = \mathcal{H} U. \quad (17)$$

It is equivalent to

$$0 = U^\dagger \mathcal{H} U - i U^\dagger \dot{U}, \quad (18)$$

comparison of Eq.(15) and Eq.(18), when considering $\mathcal{P}_N \circ \dots \circ \mathcal{P}_2 \circ \mathcal{P}_1(\mathcal{H}) = 0$, we can find the relationship between the evolution operator U and the compound picture view transformation. Thus, if the initial time is t_0 , the evolution operator of the system is

$$U(t) = e^{-i\theta_1(t)A_1} e^{-i\theta_2(t)A_2} \dots e^{-i\theta_N(t)A_N} \times e^{i\theta_N(t_0)A_N} e^{i\theta_{N-1}(t_0)A_{N-1}} \dots e^{i\theta_1(t_0)A_1}. \quad (19)$$

It can derive follow equation from Eq.(18)

$$\begin{aligned} \mathcal{L}_N \circ \dots \circ \mathcal{L}_2 \circ \mathcal{L}_1(\mathcal{H}) &= \dot{\theta}_1(t) \mathcal{L}_N \circ \dots \circ \mathcal{L}_3 \circ \mathcal{L}_2(A_1) \\ &\quad + \dot{\theta}_2(t) \mathcal{L}_N \circ \dots \circ \mathcal{L}_4 \circ \mathcal{L}_3 \\ &\quad + \dots \\ &\quad + \dot{\theta}_{N-2}(t) \mathcal{L}_N \circ \mathcal{L}_{N-1}(A_{N-2}) \\ &\quad + \dot{\theta}_{N-1}(t) \mathcal{L}_N(A_{N-1}) \\ &\quad + \dot{\theta}_N(t) A_N. \end{aligned} \quad (20)$$

In generally, by designing the parameter $\theta_1, \theta_2 \dots \theta_N$ within the evolution operator, we can control the evolution of the system's state to achieve the desired state, and the choice of parameter $\theta_1, \theta_2 \dots \theta_N$ also allows to inversion determine the control parameter $\lambda_1, \lambda_2, \dots, \lambda_n$.

B. Interconversion of GHZ state and KLM state

In this section, we combine effective Hamiltonian Eq. (11) and Lie-transform-based pulse design to create control pulses. We aim to obtain evolution operators in real form and consider them in conjunction with the effective Hamiltonian, thus we choose follow generator

$$\begin{aligned} A_1 &= i|\zeta_2\rangle\langle\zeta_1| - i|\zeta_1\rangle\langle\zeta_2|, \\ A_2 &= i|\zeta_4\rangle\langle\zeta_3| - i|\zeta_3\rangle\langle\zeta_4|, \\ A_3 &= i|\zeta_2\rangle\langle\zeta_3| - i|\zeta_3\rangle\langle\zeta_2|, \\ A_4 &= i|\zeta_4\rangle\langle\zeta_1| - i|\zeta_1\rangle\langle\zeta_4|, \\ A_5 &= i|\zeta_3\rangle\langle\zeta_1| - i|\zeta_1\rangle\langle\zeta_3|, \\ A_6 &= i|\zeta_4\rangle\langle\zeta_2| - i|\zeta_2\rangle\langle\zeta_4|, \end{aligned} \quad (21)$$

with $|\zeta_1\rangle = |000\rangle$, $|\zeta_2\rangle = |r00\rangle$, $|\zeta_3\rangle = |rr0\rangle$, $|\zeta_4\rangle = |rrr\rangle$. Obviously, effective Hamiltonian is

$$H_{eff} = \Omega'_1 A_1 + \Omega'_2 A_3 + \Omega'_3 A_2, \quad (22)$$

where $\Omega_1 = i\Omega'_1$, $\Omega_2 = -i\Omega'_2$, $\Omega_3 = i\Omega'_3$. From Eq. (20), we can derive

$$\begin{aligned} H_{eff} &= \dot{\theta}_1(t)A_1 + \dot{\theta}_2(t)\mathcal{L}_1^{-1}A_2 + \dot{\theta}_3(t)\mathcal{L}_1^{-1}\mathcal{L}_2^{-1}A_3 \\ &\quad + \dot{\theta}_4(t)\mathcal{L}_1^{-1}\mathcal{L}_2^{-1}\mathcal{L}_3^{-1}A_4 \\ &\quad + \dot{\theta}_5(t)\mathcal{L}_1^{-1}\mathcal{L}_2^{-1}\mathcal{L}_3^{-1}\mathcal{L}_4^{-1}A_5 \\ &\quad + \dot{\theta}_6(t)\mathcal{L}_1^{-1}\mathcal{L}_2^{-1}\mathcal{L}_3^{-1}\mathcal{L}_4^{-1}\mathcal{L}_5^{-1}A_6, \end{aligned} \quad (23)$$

then, the forms of parameters in control fields can be obtained

$$\begin{aligned} \Omega'_1 &= \dot{\theta}_1 + \dot{\theta}_5 \cos \theta_4 \sin \theta_3 + \dot{\theta}_6 \cos \theta_3 \sin \theta_4, \\ \Omega'_2 &= \dot{\theta}_3 \cos \theta_1 \cos \theta_2 + \dot{\theta}_4 \sin \theta_1 \sin \theta_2 \\ &\quad - \dot{\theta}_5 \cos \theta_2 \cos \theta_3 \cos \theta_4 \sin \theta_1 \\ &\quad - \dot{\theta}_6 \cos \theta_1 \sin \theta_2 \sin \theta_3 \sin \theta_4 \\ &\quad + \dot{\theta}_6 \cos \theta_1 \cos \theta_3 \cos \theta_4 \sin \theta_2 \\ &\quad + \dot{\theta}_6 \cos \theta_2 \sin \theta_1 \sin \theta_3 \sin \theta_4, \\ \Omega'_3 &= \dot{\theta}_2 - \dot{\theta}_5 \cos \theta_3 \sin \theta_4 - \dot{\theta}_6 \cos \theta_4 \sin \theta_3, \end{aligned} \quad (24)$$

and constrain conditions

$$\begin{aligned} \dot{\theta}_4 &= \dot{\theta}_3 \tan \theta_1 \tan \theta_2, \\ \dot{\theta}_5 &= \frac{2\dot{\theta}_3(\sin \theta_3 \sin \theta_4 \tan \theta_2 - \cos \theta_3 \cos \theta_4 \tan \theta_1)}{\cos 2\theta_3 + \cos 2\theta_4}, \\ \dot{\theta}_6 &= \frac{2\dot{\theta}_3(\cos \theta_3 \cos \theta_4 \tan \theta_2 - \sin \theta_3 \sin \theta_4 \tan \theta_1)}{\cos 2\theta_3 + \cos 2\theta_4}. \end{aligned} \quad (25)$$

Further, from Eq.(19), when we set $\theta_k(t_0) = 0$ ($k = 1, 2, \dots, 6$) in initial time t_0 , the real evolution operator of effective Hamiltonian (11) can be written

$$U_{eff}(t) = \begin{bmatrix} \cos \theta_1 \cos \theta_4 \cos \theta_5 - \sin \theta_1 \sin \theta_3 \sin \theta_5 & -\cos \theta_3 \cos \theta_6 \sin \theta_1 - \cos \theta_1 \sin \theta_4 \sin \theta_6 \\ \cos \theta_4 \cos \theta_5 \sin \theta_1 + \cos \theta_1 \sin \theta_3 \sin \theta_5 & \cos \theta_1 \cos \theta_3 \cos \theta_6 - \sin \theta_1 \sin \theta_4 \sin \theta_6 \\ \cos \theta_2 \cos \theta_3 \sin \theta_5 - \cos \theta_5 \sin \theta_2 \sin \theta_4 & -\cos \theta_2 \cos \theta_6 \sin \theta_3 - \cos \theta_4 \sin \theta_2 \sin \theta_6 \\ \cos \theta_2 \cos \theta_5 \sin \theta_4 + \cos \theta_3 \sin \theta_2 \sin \theta_5 & \cos \theta_2 \cos \theta_4 \sin \theta_6 - \cos \theta_6 \sin \theta_2 \sin \theta_3 \\ -\cos \theta_1 \cos \theta_4 \sin \theta_5 - \cos \theta_5 \sin \theta_1 \sin \theta_3 & \cos \theta_3 \sin \theta_1 \sin \theta_6 - \cos \theta_1 \cos \theta_6 \sin \theta_4 \\ \cos \theta_1 \cos \theta_5 \sin \theta_3 - \cos \theta_4 \sin \theta_1 \sin \theta_5 & -\cos \theta_6 \sin \theta_1 \sin \theta_4 - \cos \theta_1 \cos \theta_3 \sin \theta_6 \\ \cos \theta_2 \cos \theta_3 \cos \theta_5 + \sin \theta_2 \sin \theta_4 \sin \theta_5 & \cos \theta_2 \sin \theta_3 \sin \theta_6 - \cos \theta_4 \cos \theta_6 \sin \theta_2 \\ -\cos \theta_2 \sin \theta_4 \sin \theta_5 + \cos \theta_3 \cos \theta_5 \sin \theta_2 & \cos \theta_2 \cos \theta_4 \cos \theta_6 + \sin \theta_2 \sin \theta_3 \sin \theta_6 \end{bmatrix} \quad (26)$$

For simplicity, assume that the system initially starts in state $|\zeta_1\rangle$. By controlling the system with the evolution operator U_{eff} of effective Hamiltonian, we can determine the state of

the system at any given point in time

$$U_{eff}|\zeta_1\rangle = \begin{pmatrix} \cos \theta_1 \cos \theta_4 \cos \theta_5 - \sin \theta_1 \sin \theta_3 \sin \theta_5 \\ \cos \theta_1 \sin \theta_3 \sin \theta_5 + \sin \theta_1 \cos \theta_4 \cos \theta_5 \\ \cos \theta_2 \cos \theta_3 \sin \theta_5 - \sin \theta_2 \sin \theta_4 \cos \theta_5 \\ \sin \theta_2 \cos \theta_3 \sin \theta_5 + \cos \theta_2 \sin \theta_4 \cos \theta_5 \end{pmatrix}. \quad (27)$$

Clearly, from Eq.(27), by determining the boundary conditions for θ_k ($k = 1, 2, \dots, 6$), we can achieve the interconversion between GHZ state and KLM state. We have assumed that the initial state at time $t = t_0$ is $|\zeta_1\rangle = |000\rangle$. Let's further assume that at time $t = t_{ghz}$, the system evolves into the GHZ state, and at $t = t_{klm}$, it evolves into the KLM state. Specifically speaking, when the boundary conditions satisfy

$$\begin{aligned}\theta_1(t_{ghz}) &= \theta_2(t_{ghz}) = \theta_5(t_{ghz}) = 0, \\ \theta_4(t_{ghz}) &= \frac{\pi}{4},\end{aligned}\quad (28)$$

the system will evolve to the $|GHZ\rangle$ state. When the condition is set to

$$\begin{aligned}\theta_1(t_{klm}) &= -\frac{\pi}{4}, \quad \theta_2(t_{klm}) = \frac{\pi}{4}, \\ \theta_3(t_{klm}) &= \frac{\pi}{4}, \quad \theta_5(t_{klm}) = \frac{\pi}{2},\end{aligned}\quad (29)$$

the system will evolve to the $|KLM\rangle$ state, where $|GHZ\rangle = (|\zeta_1\rangle + |\zeta_4\rangle)/\sqrt{2} = (|000\rangle + |rrr\rangle)/\sqrt{2}$, and $|KLM\rangle = (|\zeta_1\rangle + |\zeta_2\rangle + |\zeta_3\rangle + |\zeta_4\rangle)/2 = (|000\rangle + |r00\rangle + |rr0\rangle + |rrr\rangle)/2$.

Our focus is on the evolution time between t_{ghz} and t_{klm} . When we consider GHZ state to KLM state, we can conveniently set $t_{ghz} = 0$ and $t_{klm} = T$. Through Eq.(28) and (29), we can find that θ_1, θ_2 , and θ_5 are boundary conditions fixed at both ends, and θ_3 and θ_4 are boundary conditions fixed on one side. The boundary conditions for θ_6 are free at both ends. Eq.(25) represent the relationship between these parameters. Taking into account the above considerations and no singularities in equation, design parameters can be choose

$$\begin{aligned}\theta_1(t) &= -\frac{\pi}{16} \left(1 - \cos \frac{\pi t}{T}\right)^2, \\ \theta_2(t) &= \left(\sin \frac{\pi t}{2T}\right)^2 \left(1 - \cos \frac{\pi t}{T}\right), \\ \theta_3(t) &= \frac{\pi}{4} + \mathcal{C} \sin \left(\frac{\pi(t-T)}{T}\right)^2,\end{aligned}\quad (30)$$

where \mathcal{C} is a coefficient to be determined. By numerically calculating Eq.(25), we obtain $\mathcal{C} = 2.4084$ with boundary conditions $\theta_5(0) = 0$ and $\theta_5(T) = \frac{\pi}{2}$. To derive an expression for $\Omega'_1, \Omega'_2, \Omega'_3$, we add $\theta_6(0) = 0$. Through numerical computation, we can then determine $\Omega'_1, \Omega'_2, \Omega'_3$, which exhibits the form shape in Fig.2(a). Similarly, when we consider KLM state to GHZ state, we only need to let $t_{klm} = 0$, $t_{ghz} = T$. We can easily setting

$$\begin{aligned}\theta_1(t) &= -\frac{\pi}{16} \left(1 - \cos \frac{\pi(t-T)}{T}\right)^2, \\ \theta_2(t) &= \left(\sin \frac{\pi(t-T)}{2T}\right)^2 \left(1 - \cos \frac{\pi(t-T)}{T}\right), \\ \theta_3(t) &= \frac{\pi}{4} + \mathcal{C} \sin \left(\frac{\pi t}{T}\right)^2.\end{aligned}\quad (31)$$

And the shape of the control pulse obtained is shown in Fig.2(b).

To demonstrate the effectiveness of our pulse design, we simulate effective Hamiltonian (11) and plot the fidelity of the interconversion GHZ state to KLM state as shown in Fig.2(c) and 2(d), respectively. We can find, this parameter choice has a high fidelity for the effective Hamiltonian.

IV. NUMERICAL SIMULATION AND ANALYSES

In this section, we proceed with numerical simulations and analyses. By employing parameters that can be realized experimentally, this study further explores the impact of various decoherence mechanisms on the stability of quantum state evolution. This step aims to verify the effectiveness and robustness of our scheme under realistic experimental conditions.

It is well known that if a unitary transformation is performed from an old picture to a new picture, the quantum state will undergo a phase change. The implementation of the conversion between GHZ state and KLM state takes place under the new picture as defined by Eq. (5). If discussed in the old picture, a state would experience a phase transformation. Specifically, if a state can be described as $|\psi\rangle$ in the new picture, when transformed back to the original picture, it will becomes to $\mathcal{R}|\psi\rangle$. Although there is a change in phase, once we determine the value of VT , we can derive the specific phase of the final state. What we are concerned with is the probability amplitude of the state. Based on this consideration, we define the fidelity at the time t in the original picture as $F = |\langle\psi|\mathcal{R}^\dagger\rho(t)\mathcal{R}|\psi\rangle|$, where $\rho(t)$ is the density operator in original picture. So, we define the fidelity of obtaining the KLM state from the GHZ state as $F_1 = |\langle KLM|\mathcal{R}^\dagger\rho(t)\mathcal{R}|KLM\rangle|$. Similarly, the fidelity of the GHZ state is obtained from the KLM state is $F_2 = |\langle GHZ|\mathcal{R}^\dagger\rho(t)\mathcal{R}|GHZ\rangle|$. We performed numerical simulations with the Hamiltonian(2), the fidelities F_1 and F_2 are shown in Fig.3, where we have chosen the parameter $V = 100\pi/T$, which clearly satisfies the $V \gg \text{Max}\{|\Omega_1|, |\Omega_2|, |\Omega_3|\} \approx 11.4/T$. Numerical simulation results show that the fidelities are more than 99.7% at the moment of T .

Considering the effects of thermal noise, dephasing, and spontaneous emission on the present scheme, we conducted numerical simulations on the fidelities of interconversions between GHZ state and KLM state using the master equation [47]

$$\begin{aligned}\dot{\rho} &= -i[H(t), \rho] + D_{\text{deph}}(\rho) + D_{\text{therm}}(\rho), \\ D_{\text{deph}} &= \sum_{k=1}^3 \left[L_k \rho L_k^\dagger - \frac{1}{2} (L_k^\dagger L_k \rho + \rho L_k^\dagger L_k) \right], \\ D_{\text{therm}} &= \sum_{k=4}^6 \left\{ (\bar{n} + 1) \left[L_k \rho L_k^\dagger - \frac{1}{2} (L_k^\dagger L_k \rho + \rho L_k^\dagger L_k) \right] \right. \\ &\quad \left. + \bar{n} \left[L_k^\dagger \rho L_k - \frac{1}{2} (L_k L_k^\dagger \rho + \rho L_k L_k^\dagger) \right] \right\},\end{aligned}\quad (32)$$

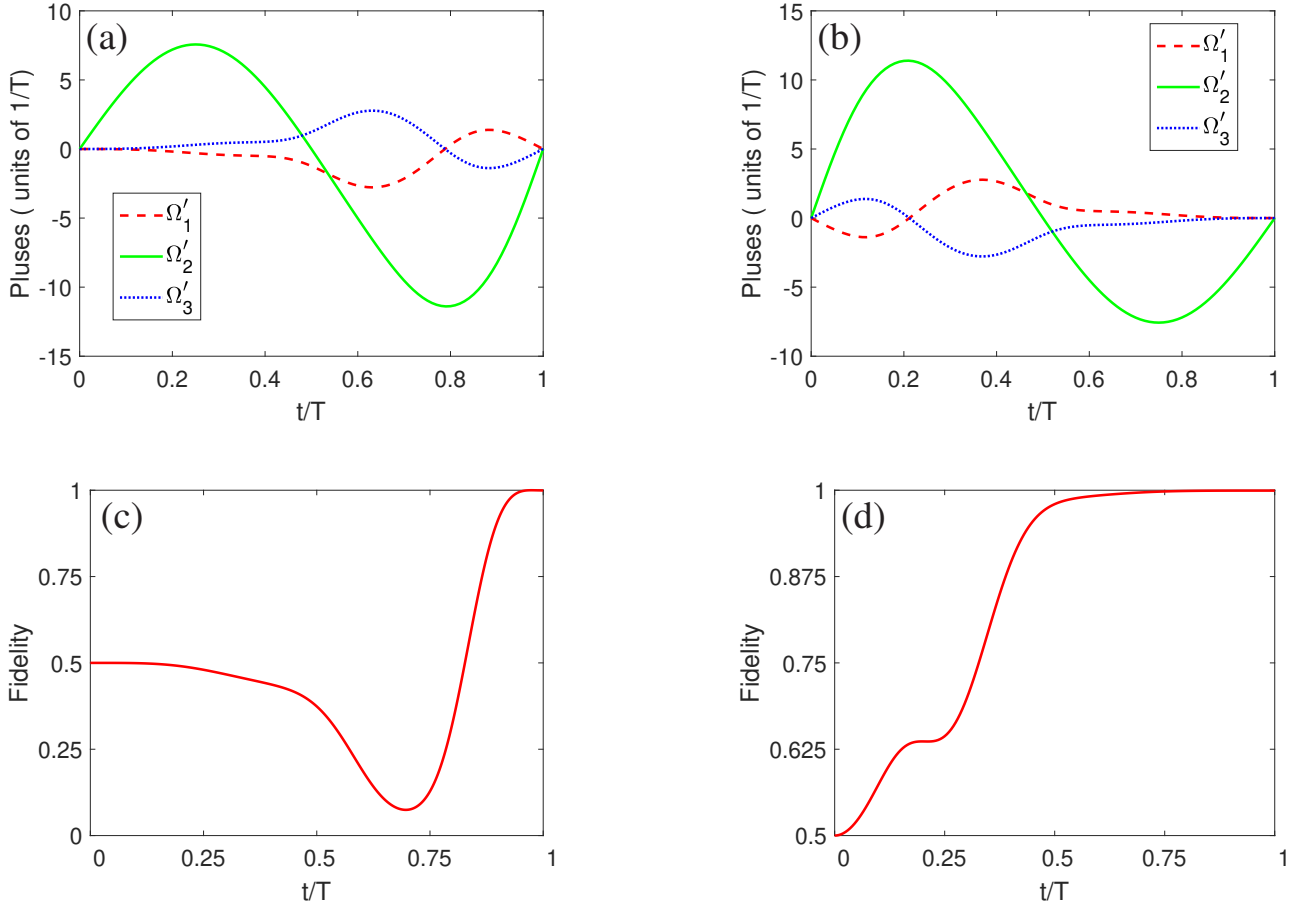


FIG. 2: (a) Rabi frequencies $\Omega'_1, \Omega'_2, \Omega'_3$ (versus t/T) for conversion of GHZ to KLM state. (b) Rabi frequencies $\Omega'_1, \Omega'_2, \Omega'_3$ (versus t/T) for conversion of KLM to GHZ state. (c) The fidelity of GHZ to KLM state (versus t/T) by simulating the Hamiltonian(11). (d) The fidelity of KLM to GHZ state (versus t/T) by simulating the Hamiltonian(11).

where \bar{n} is the average number of thermal phonons which is set in a scope as $0 \sim 1$, when considering the Bose-Einstein distribution, this average phonon number is calculated by $1/(e^{\frac{\hbar\omega}{k_B T}} - 1)$, which is related to the temperature of the environment T and the frequency ω of thermal noise. L_k ($k = 1, 2, 3, 4, 5, 6$) are the Lindblad operators, which are

$$\begin{aligned}
 L_1 &= \sqrt{\gamma_1} (|r\rangle_1 \langle r| - |0\rangle_1 \langle 0|), \\
 L_2 &= \sqrt{\gamma_2} (|r\rangle_2 \langle r| - |0\rangle_2 \langle 0|), \\
 L_3 &= \sqrt{\gamma_3} (|r\rangle_3 \langle r| - |0\rangle_3 \langle 0|), \\
 L_4 &= \sqrt{\Gamma_1} |0\rangle_1 \langle r|, \\
 L_5 &= \sqrt{\Gamma_2} |0\rangle_2 \langle r|, \\
 L_6 &= \sqrt{\Gamma_3} |0\rangle_3 \langle r|,
 \end{aligned} \tag{33}$$

Γ_k is atomic spontaneous emission rate from $|r\rangle$ to $|0\rangle$, γ_k being the dephasing rate of the k th atom. For simplicity, here we set $\Gamma_1 = \Gamma_2 = \Gamma_3 = \Gamma$, $\gamma_1 = \gamma_2 = \gamma_3 = \gamma$. In Fig. 4, we illustrate the effects of atomic spontaneous emission Γ and dephasing rates γ on fidelity (note, Γ, γ unite of $1/T$), where we have set the average number of thermal phonons

$\bar{n} = 0$. Through Fig. 4, we can see that this scheme demonstrates robustness against atomic spontaneous emission and dephasing rate.

Next, we plotted the fidelity as it varies with atomic spontaneous emission and the average number of thermal photons as shown in Fig. 5, even when $\bar{n} = 1$ and $\Gamma = 0.02$ (unites of $1/T$), the fidelity remains above 91.5%. Therefore, we can prove that the scheme is robust against spontaneous emission and the thermal noise. Here, we consider the total evolutionary time $T = 20\mu s$, which is still much less than the reported coherence time of Rydberg atom. By considering a group of parameters that are feasible for experiments, $\Gamma = 1\text{kHz}$, $\gamma = 1\text{kHz}$ (i.e. 0.02 unite of $1/T$) and experimental temperature is $20\mu K$ [48], assuming the frequency of thermal noise as $\omega = 2\pi \times 1\text{MHz}$ (i.e. $\bar{n} \sim 0.1$). It can obtain $F_1 = 91.16\%$ and $F_2 = 91.17\%$. This indicates the scheme demonstrate robustness against decoherence.

In order to further explore the robustness of the protocol under realistic experimental conditions, we will next introduce a factor that is closer to the actual situation, i.e. Gaussian white noise. This noise model will be applied to the control field to simulate the unavoidable environmental dis-

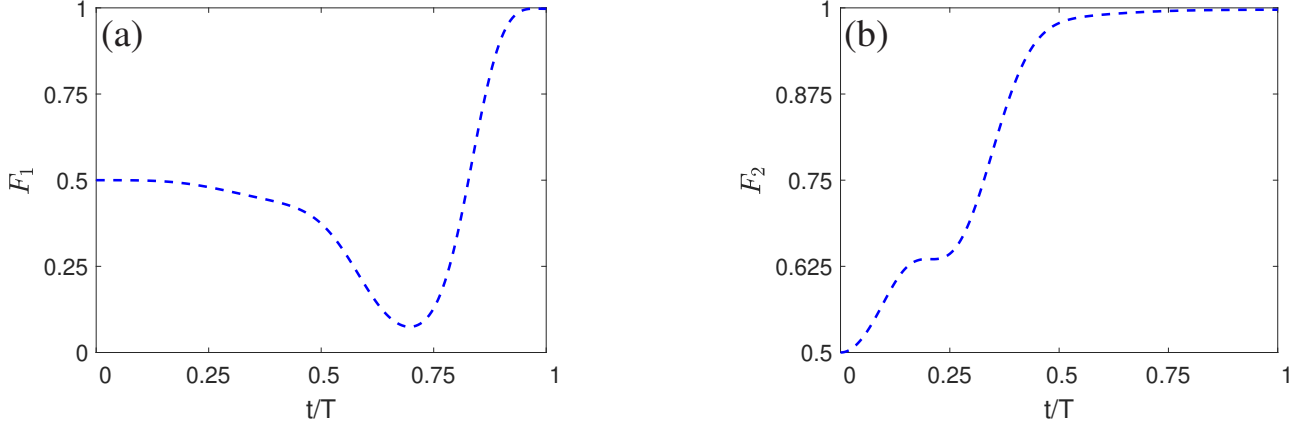


FIG. 3: (a) The fidelity F_1 versus t/T . (b) The fidelity F_2 versus t/T

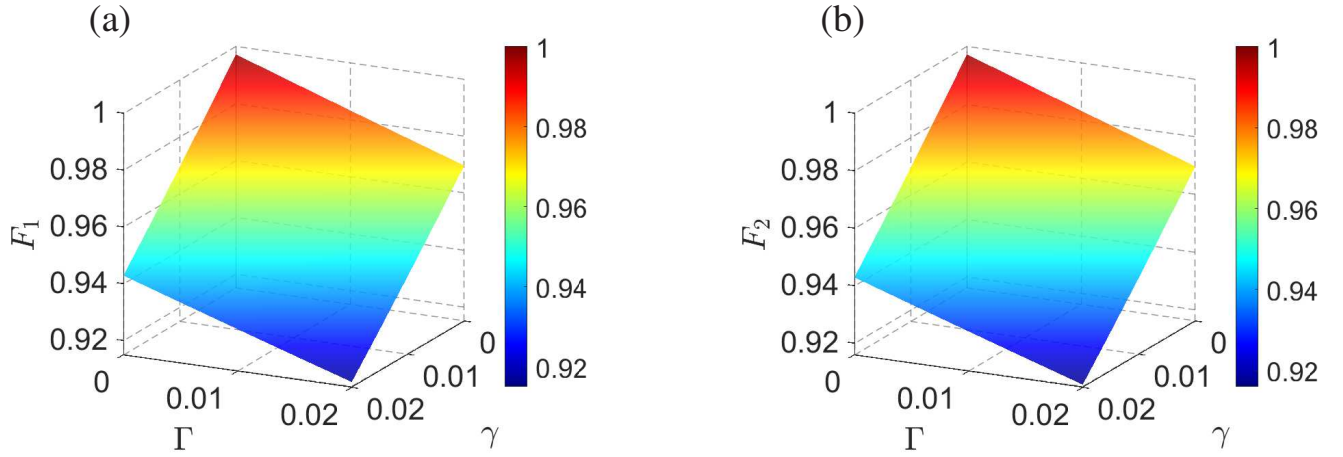


FIG. 4: The fidelity (a) F_1 , (b) F_2 versus the decoherence of spontaneous emission Γ and dephasing γ (Γ, γ unite of $1/T$).

turbances and systematic errors in the experiment. By introducing Gaussian white noise into our control scheme, we evaluate the effect of noise on system evolution and final state fidelities. Then additive white Gaussian noise (AWGN) leads to the noisy control field as

$$\Omega_k^{no} = \Omega_k + \text{Awgn}(\Omega_k, \kappa), \quad (34)$$

where $\text{Awgn}(\Omega_k, \kappa)$ denotes a function-generating AWGN with signal-to-noise ratio (SNR) κ for Ω_k . We performed ten separate simulations for each different SNR, the results are shown in the Fig. 6. We can see that even with SNR $\kappa = 10$, the fidelities is still above 97%.

As discussed earlier, our scheme requires the selection of a suitable detuning δ_k . In the following, we discuss the effect of a slight mismatch in the value of δ_k on the final fidelity,

$$\delta'_k = (1 + \eta)\delta_k, \quad (35)$$

where η is the coefficient of the mismatch on detuning. By substituting the δ'_k for δ_k , the numerical simulation results are shown in Fig. 7. We can find that the scheme has a relatively high requirement for Rabi frequency detuning, and the

fidelity have 0.81 when the deviation is 0.03%. Considering that the value of V is very large, the existing experimental techniques are very fine [49–51], which can achieve a high degree of stable control of the laser frequency, and can maintain a low frequency drift even when it is far away from the atomic resonance line, for example, the drift of the detuning locked away from the atomic resonance line is less than 1 Mhz/h. Therefore, this scheme exhibits a certain level of robustness to detuning mismatches in experimental settings.

V. SUMMARY

In summary, we have proposed a scheme to realize the interconversion of GHZ and KLM state of atomic system. We simplify the dynamics by utilizing the energy level shift terms of the Rydberg atomic system, the effective Hamiltonian for the physical model can ultimately be simplified to a four-level Hamiltonian with basis $\{|000\rangle, |r00\rangle, |rr0\rangle, |rrr\rangle\}$. In this evolutionary space, we implement the interconversion of GHZ and KLM state by Lie-transform-based pulse design. We performed numerical simulations to evalu-

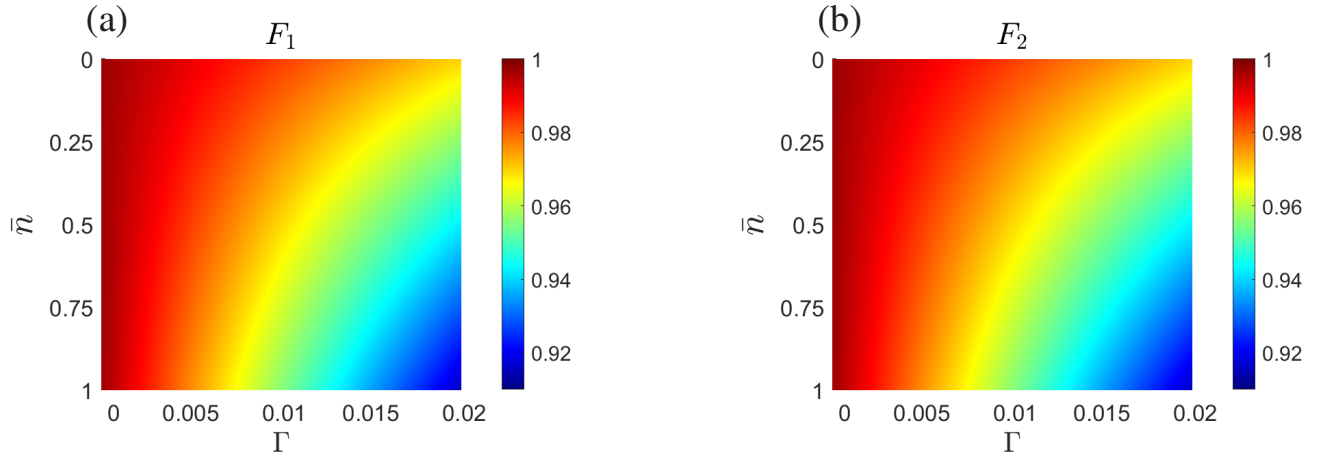


FIG. 5: The fidelity (a) F_1 , (b) F_2 versus the spontaneous emission Γ and the average number of thermal phonons \bar{n} .

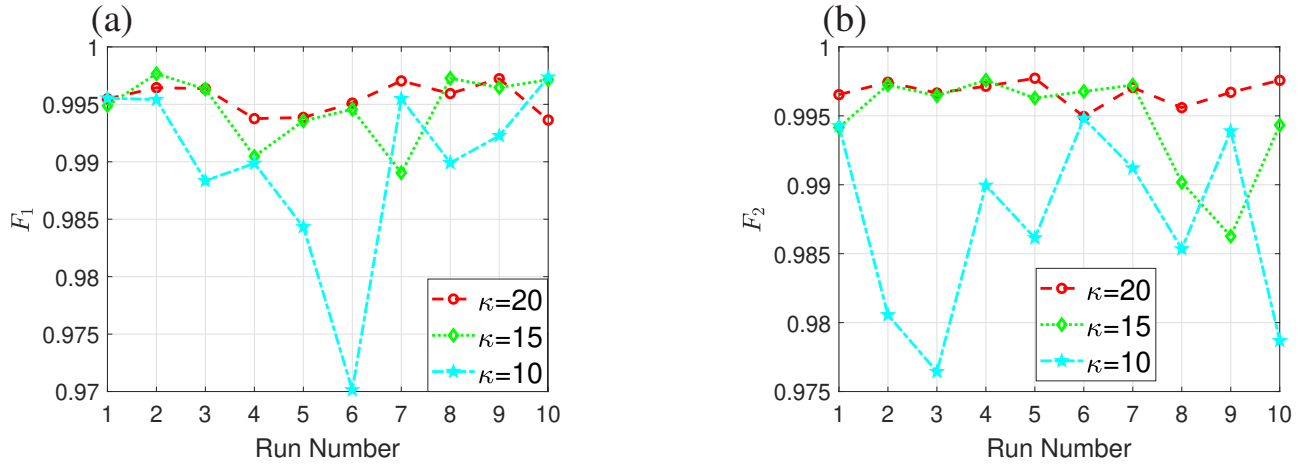


FIG. 6: (a) The fidelity F_1 of the conversion from GHZ to KLM state under AWGN versus run number. (b) The fidelity F_2 of the conversion from KLM to GHZ state under AWGN versus run number.

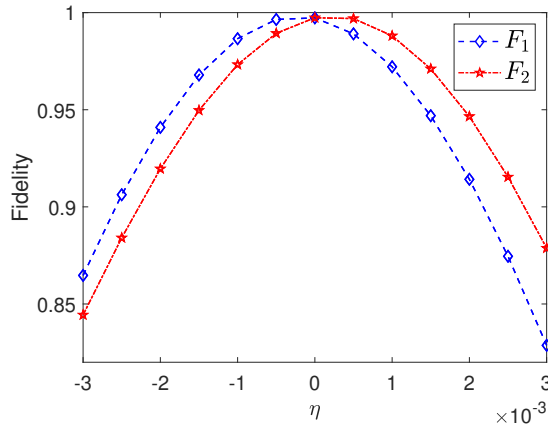


FIG. 7: Fidelities F_1 and F_2 versus mismatch on detuning η with blue diamond line and red astroid line, respectively

mal noise, dephasing and spontaneous emission, the numerical simulation results show that the scheme is robust against various decoherence. In addition, we analyze the effect of Gaussian noise and mismatch of detuning on the results. In a nutshell, this scheme features deterministic and reversible state conversions, and has high fidelities in both directions. We believe this paper will offer fresh insights and potentially introduce new ideas, contributing to the advancement of quantum information exploration.

ACKNOWLEDGMENTS

This work was supported by the Program of the Educational Office of LiaoNing Province of China (Grant Nos. LJKZ1015, LJ2020005, LJKZZ20220120), the Natural Science Foundation of LiaoNing Province (Grant Nos. 2020-BS-234, 2021-MS-317, 2022-MS-372), the Program of Liaoning BaiQianWan Talents Program (Grant No. 2021921096).

ate the influence of various decoherence factors, such as ther-

Appendix

In this section, we are going to explain in detail why fidelity is defined with the addition of \mathcal{R} . We start with unitary transformations. A unitary transformation is a transformation that preserves the inner product. For Schrödinger equation ($\hbar = 1$)

$$i \frac{\partial |\psi\rangle}{\partial t} = H |\psi\rangle \quad (\text{A.1})$$

There exists a unitary operator \mathcal{R}^\dagger acting on $|\psi\rangle$ such that

$$\mathcal{R}^\dagger |\psi\rangle = |\psi'\rangle \quad (\text{A.2})$$

It is equivalent to

$$|\psi\rangle = \mathcal{R} |\psi'\rangle \quad (\text{A.3})$$

$|\psi'\rangle$ also follow the Schrödinger equation, assume it has follow form in new picture

$$i \frac{\partial |\psi'\rangle}{\partial t} = H' |\psi'\rangle \quad (\text{A.4})$$

Substituting Eq.(A.3) into Eq.(A.1), can be obtain

$$\begin{aligned} i \frac{\partial (\mathcal{R} |\psi'\rangle)}{\partial t} &= H (\mathcal{R} |\psi'\rangle) \\ i \frac{\partial \mathcal{R}}{\partial t} |\psi'\rangle + i \mathcal{R} \frac{\partial |\psi'\rangle}{\partial t} &= H \mathcal{R} |\psi'\rangle \end{aligned} \quad (\text{A.5})$$

left multiply \mathcal{R}^\dagger ,

$$\begin{aligned} i \mathcal{R}^\dagger \frac{\partial \mathcal{R}}{\partial t} |\psi'\rangle + i \frac{\partial |\psi'\rangle}{\partial t} &= \mathcal{R}^\dagger H \mathcal{R} |\psi'\rangle \\ i \frac{\partial |\psi'\rangle}{\partial t} &= \left(\mathcal{R}^\dagger H \mathcal{R} - i \mathcal{R}^\dagger \frac{\partial \mathcal{R}}{\partial t} \right) |\psi'\rangle \end{aligned} \quad (\text{A.6})$$

Comparison of the above results Eq.(A.6) and Eq.(A.4), we can obtain the relationship between the Hamiltonian H' in the new picture after performing the unitary transformation \mathcal{R} and the Hamiltonian H in the original picture

$$H' = \mathcal{R}^\dagger H \mathcal{R} - i \mathcal{R}^\dagger \frac{\partial \mathcal{R}}{\partial t} \quad (\text{A.7})$$

This is the origin of Eq.(5) in the main text.

If a unitary transformation \mathcal{R} is performed from an old picture to a new picture, density operator also undergoes a unitary transformation

$$\rho'(t) = |\psi'(t)\rangle \langle \psi'(t)| = \mathcal{R}^\dagger |\psi(t)\rangle \langle \psi(t)| \mathcal{R} = \mathcal{R}^\dagger \rho(t) \mathcal{R} \quad (\text{A.8})$$

where ' denotes representation in new picture. Since state $|\varphi\rangle$ is represented in the new picture. In the new picture according to the general definition of fidelity $\langle \varphi | \rho'(t) | \varphi \rangle$, but if I want to use the density operator $\rho(t)$ in the old picture, the fidelity is $\langle \varphi | \mathcal{R}^\dagger \rho(t) \mathcal{R} | \varphi \rangle$. Or it can be understood as us performing the inverse transformation from the new picture $|\varphi\rangle$ to the old picture $\mathcal{R} |\varphi\rangle$. This is why we define fidelity in this way.

Interestingly, many articles assume the above knowledge is commonly accepted, but they do not specify it explicitly. They do not differentiate between the new picture and the old picture, for example: Ref [13, 41], They define fidelity as $\langle \varphi | \rho | \varphi \rangle$, but their numerical simulations yield $\langle \varphi | \rho'(t) | \varphi \rangle = \langle \varphi | \mathcal{R}^\dagger \rho(t) \mathcal{R} | \varphi \rangle$. The sketches I drew based on their articles is as follows If fidelity is defined as described in their articles, it would correspond to curve N. Their articles curve is R because they implicitly assume a rotation has been performed. The reason I am writing so much to emphasize that my definition here is correct and not a mistake; it is reasonable.

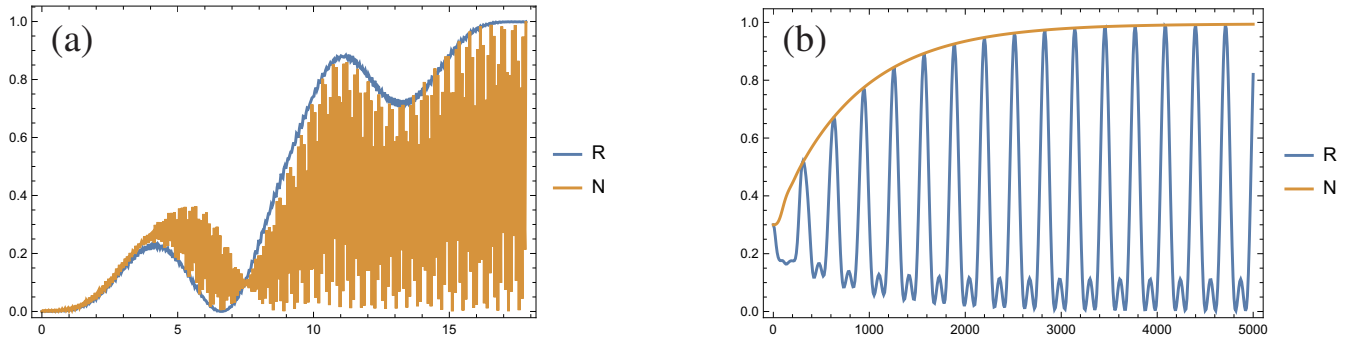


FIG. 8: sketch(a) follow Figure 3(c) in Ref[13] sketch(b) follow Figure 2(c) in Ref[41].

- [3] S. Pirandola, J. Eisert, C. Weedbrook, A. Furusawa, and S. L. Braunstein, *Nat. Photonics* **9**, 641 652 (2015).
- [4] X. M. Hu, Y. Guo, B. H. Liu, C. F. Li, and G. C. Guo, *Nature Reviews Physics* **5**, 339 353 (2023).
- [5] V. Scarani, H. Bechmann Pasquinucci, N. J. Cerf, M. Dušek, N. Lütkenhaus, and M. Peev, *Rev. Mod. Phys.* **81**, 1301 1350 (2009).
- [6] F. Xu, X. Ma, Q. Zhang, H. K. Lo, and J. W. Pan, *Rev. Mod. Phys.* **92**, 025002 (2020).
- [7] D. J. Bernstein and T. Lange, *Nature* **549**, 188 (2017).
- [8] S. Pirandola, U. L. Andersen, L. Banchi, M. Berta, D. Bunandar, R. Colbeck, D. Englund, T. Gehring, C. Lupo, C. Ottaviani, *et al.*, *Adv. Opt. Photonics* **12**, 1012 1236 (2020).
- [9] C. Portmann and R. Renner, *Rev. Mod. Phys.* **94**, 025008 (2022).
- [10] H. J. Briegel, D. E. Browne, W. Dür, R. Raussendorf, and M. Van den Nest, *Nat. Phys.* **5**, 19 26 (2009).
- [11] M. Horowitz and E. Grumblin, *Quantum computing: progress and prospects* (National Academies Press, 2019).
- [12] T. Albash and D. A. Lidar, *Rev. Mod. Phys.* **90**, 015002 (2018).
- [13] R. H. Zheng, Y. H. Kang, D. Ran, Z. C. Shi, and Y. Xia, *Phys. Rev. A* **101**, 012345 (2020).
- [14] J. Song, X. D. Sun, Q. X. Mu, L. L. Zhang, Y. Xia, and H. S. Song, *Phys. Rev. A* **88**, 024305 (2013).
- [15] X. Q. Shao, F. Liu, X. W. Xue, W. L. Mu, and W. Li, *Phys. Rev. Appl.* **20**, 014014 (2023).
- [16] S. Liu, Y. H. Chen, Y. Wang, Y. H. Kang, Z. C. Shi, J. Song, and Y. Xia, *Phys. Rev. A* **106**, 042430 (2022).
- [17] W. Y. Zhang, C. Q. Wang, Y. Q. Ji, Q. P. Shao, J. P. Wang, J. Wang, L. P. Yang, L. Dong, and X. M. Xiu, *Advanced Quantum Technologies* **7**, 2300140 (2024).
- [18] Y. Q. Ji, X. Q. Shao, and X. X. Yi, *Opt. Express* **25**, 15806 15817 (2017).
- [19] J. L. Wu, S. L. Su, X. Ji, and S. Zhang, *Ann. Phys.* **386**, 34 43 (2017).
- [20] T. P. Gujarati, *Phys. Rev. A* **98**, 062326 (2018).
- [21] Y. Q. Ji, Y. L. Liu, S. J. Zhou, X. M. Xiu, L. Dong, H. K. Dong, Y. J. Gao, and X. X. Yi, *Phys. Rev. A* **99**, 023808 (2019).
- [22] Y. H. Kang, Z. C. Shi, B. H. Huang, J. Song, and Y. Xia, *Phys. Rev. A* **100**, 012332 (2019).
- [23] C. P. Shen, X. M. Xiu, L. Dong, X. Y. Zhu, L. Chen, E. Liang, L. L. Yan, and S. L. Su, *Ann. Phys.* **531**, 1900160 (2019).
- [24] M. Saffman, T. G. Walker, and K. Mølmer, *Rev. Mod. Phys.* **82**, 2313 2363 (2010).
- [25] N. Šibalić and C. S. Adams, *Rydberg Physics*, 2399-2891 (IOP Publishing, 2018).
- [26] X.-F. Shi, *Quantum Sci. Technol.* **7**, 023002.
- [27] A. Gaëtan, Y. Miroshnychenko, T. Wilk, A. Chotia, M. Viteau, D. Comparat, P. Pillet, A. Browaeys, and P. Grangier, *Nat. Phys.* **5**, 115 118 (2009).
- [28] E. Urban, T. A. Johnson, T. Henage, L. Isenhower, D. Yavuz, T. Walker, and M. Saffman, *Nat. Phys.* **5**, 110 114 (2009).
- [29] X. Q. Shao, D. X. Li, Y. Q. Ji, J. H. Wu, and X. X. Yi, *Phys. Rev. A* **96**, 012328 (2017).
- [30] T. Amthor, C. Giese, C. S. Hofmann, and M. Weidemüller, *Phys. Rev. Lett.* **104**, 013001 (2010).
- [31] S. L. Su, F. Q. Guo, J. L. Wu, Z. Jin, X. Q. Shao, and S. Zhang, *Europhys. Lett.* **131**, 53001 (2020).
- [32] S. L. Su and W. Li, *Phys. Rev. A* **104**, 033716 (2021).
- [33] Y. L. Liu, Y. Q. Ji, X. Han, W. X. Cui, S. Zhang, and H. F. Wang, *Adv. Quantum Technol.* **6**, 2200173 (2023).
- [34] T. Haase, G. Alber, and V. M. Stojanović, *Phys. Rev. A* **103**, 032427 (2021).
- [35] E. Knill, R. Laflamme, and G. J. Milburn, *Nature* **409**, 46 52 (2001).
- [36] K. Lemr, A. Černoč, J. Soubusta, and J. Fiurášek, *Phys. Rev. A* **81**, 012321 (2010).
- [37] R. Okamoto, J. L. O'Brien, H. F. Hofmann, and S. Takeuchi, *Proc. Natl. Acad. Sci.* **108**, 10067 10071 (2011).
- [38] L. Y. Cheng, H. F. Wang, S. Zhang, and K. H. Yeon, *JOSA B* **29**, 1584 1588 (2012).
- [39] Y. Q. Ji, H. Li, Y. L. Liu, D. W. Zhang, X. J. Zhou, R. J. Xiao, L. Dong, and X. M. Xiu, *Laser Phys. Lett.* **17**, 085202 (2020).
- [40] C. P. Shen, X. F. Gu, Q. Guo, X. Y. Zhu, S. L. Su, and E. Liang, *JOSA B* **35**, 694 701 (2018).
- [41] D. X. Li, X. Q. Shao, J. H. Wu, X. Yi, and T. Y. Zheng, *Opt. Express* **26**, 2292 2302 (2018).
- [42] R. H. Zheng, Y. Xiao, S. L. Su, Y. H. Chen, Z. C. Shi, J. Song, Y. Xia, and S. B. Zheng, *Phys. Rev. A* **103**, 052402 (2021).
- [43] Y. H. Chen, Y. Xia, J. Song, and Q. Q. Chen, *Sci. Rep.* **5**, 15616 (2015).
- [44] J. L. Wu, C. Song, J. Xu, L. Yu, X. Ji, and S. Zhang, *Quantum Inf. Process.* **15**, 3663 (2016).
- [45] R. Li, S. He, Z.-J. Meng, Z. Jin, and W.-J. Gong, *Chin. Phys. Lett.* **40**, 060302 (2023).
- [46] Y. H. Kang, Y. H. Chen, Z. C. Shi, B. H. Huang, J. Song, and Y. Xia, *Phys. Rev. A* **97**, 033407 (2018).
- [47] I. Medina and F. L. Semião, *Phys. Rev. A* **100**, 012103 (2019).
- [48] J. D. Pritchard, D. Maxwell, A. Gauguier, K. J. Weatherill, M. P. A. Jones, and C. S. Adams, *Phys. Rev. Lett.* **105**, 193603 (2010).
- [49] A. L. Marchant, S. Händel, T. P. Wiles, S. A. Hopkins, C. S. Adams, and S. L. Cornish, *Opt. Lett.* **36**, 64 66 (2011).
- [50] R. Vijay, C. Macklin, D. Slichter, S. Weber, K. Murch, R. Naik, A. N. Korotkov, and I. Siddiqi, *Nature* **490**, 77 80

- (2012).
- [51] C. Liu, Z. Yue, Z. Xu, M. Ding, and Y. Zhai, *Appl. Sci.* **10**, 3255 (2020).